Chimpanzee super strength and human skeletal muscle evolution

Matthew C. O'Neill[a,1], Brian R. Umberger[b], Nicholas B. Holowka[c], Susan G. Larson[d], and Peter J. Reiser[e]

[a]Department of Basic Medical Sciences, University of Arizona College of Medicine–Phoenix, Phoenix, AZ 85004; [b]Department of Kinesiology, University of Massachusetts, Amherst, MA 01003; [c]Department of Human Evolutionary Biology, Harvard University, Cambridge, MA 02138; [d]Department of Anatomical Sciences, Stony Brook University School of Medicine, Stony Brook, NY 11794; and [e]Division of Biosciences, The Ohio State University College of Dentistry, Columbus, OH 43210

Edited by Jill M. Slade, Michigan State University, East Lansing, MI, and accepted by Editorial Board Member C. O. Lovejoy March 31, 2017 (received for review November 29, 2016)

Since at least the 1920s, it has been reported that common chimpanzees (*Pan troglodytes*) differ from humans in being capable of exceptional feats of "super strength," both in the wild and in captive environments. A mix of anecdotal and more controlled studies provides some support for this view; however, a critical review of available data suggests that chimpanzee mass-specific muscular performance is a more modest 1.5 times greater than humans on average. Hypotheses for the muscular basis of this performance differential have included greater isometric force-generating capabilities, faster maximum shortening velocities, and/or a difference in myosin heavy chain (MHC) isoform content in chimpanzee relative to human skeletal muscle. Here, we show that chimpanzee muscle is similar to human muscle in its single-fiber contractile properties, but exhibits a much higher fraction of MHC II isoforms. Unlike humans, chimpanzee muscle is composed of ∼67% fast-twitch fibers (MHC IIa+IId). Computer simulations of species-specific whole-muscle models indicate that maximum dynamic force and power output is 1.35 times higher in a chimpanzee muscle than a human muscle of similar size. Thus, the superior mass-specific muscular performance of chimpanzees does not stem from differences in isometric force-generating capabilities or maximum shortening velocities—as has long been suggested—but rather is due in part to differences in MHC isoform content and fiber length. We propose that the hominin lineage experienced a decline in maximum dynamic force and power output during the past 7–8 million years in response to selection for repetitive, low-cost contractile behavior.

chimpanzee | human | muscle | myosin heavy chain | muscle modeling

Modern humans—with some exceptions—are often characterized as a weak and unathletic species compared with our closest living relatives, the chimpanzees. Whereas chimpanzees are proficient tree climbers and arborealists (1), our hominin ancestors gave up a reliance on the forest canopy after the emergence of the genus *Homo* (2). Subsequent evolution in brain size (3) and cognition as well as advancements in tools and other material culture (4, 5) have reduced our strict dependence on muscular strength for survival and fitness.

Since at least the 1920s, both anecdotal reports and more controlled experiments have indicated that the strength of a chimpanzee can exceed that of a human (6–12). This has led to the now long-standing proposal that chimpanzees are "super strong" compared with humans. A critical review of experiments (i.e., pulling and jumping tasks) carried out between 1923 and 2014 suggests that chimpanzee mass-specific muscular performance consistently exceeds that of humans, with a differential of about 1.5 times, on average (*SI Appendix*, *SI Discussion*). Hypotheses for the muscular basis of the chimpanzee–human performance differential have included higher isometric force-producing capabilities (6–8, 11), faster maximum shortening velocities (7, 11), and/or a different distribution of myosin heavy chain (MHC) isoforms than human skeletal muscle (10, 11). However, to date there have been no direct measurements of these parameters in the skeletal muscle of chimpanzees. Yet, if one or more of these hypotheses are correct, it would indicate a significant (and previously unappreciated) evolutionary shift in the force and/or power-producing capabilities of skeletal muscle in either *Pan* or *Homo* since these two lineages diverged about 7–8 million years ago (Mya) (13).

In this study, we present direct measurements of single-fiber contractile properties and MHC isoform distributions of chimpanzee skeletal muscle to test these hypotheses. We compare our chimpanzee data to similar data from humans and a wide range of other terrestrial mammals. The single-fiber and MHC datasets are then used to parameterize chimpanzee and human muscle models. Computer simulation of these models under matched contractile conditions permit a controlled comparison of chimpanzee and human muscular performance capabilities. Based on our results, we suggest that the maximum dynamic force and power-producing capabilities of skeletal muscle has declined during the past 7–8 million years of hominin evolution, likely due to selection for repetitive, low-cost contractile behavior.

Results

Using an isolated muscle fiber preparation, we directly measured the maximum isometric force and maximum shortening velocity of the skeletal muscle of the common chimpanzee (*Pan troglodytes*). Data were collected at 15 °C from fibers containing pure MHC I, IIa, and IId isoforms. The maximum isometric force (P_o) of chimpanzee skeletal muscle ranged from 96 $kN{\cdot}m^{-2}$ to 150 $kN{\cdot}m^{-2}$, and the maximum shortening velocity (V_o) ranged from 0.64 to 4.96 $L{\cdot}s^{-1}$, depending on MHC type (Fig. 1

Significance

Chimpanzee "super strength" has been widely reported since the 1920s although a critical review of the available data suggests that the chimpanzee–human muscular performance differential is only ∼1.5 times. Some hypothesize that this differential reflects underlying differences in muscle mechanics. Here, we present direct measurements of chimpanzee skeletal muscle properties in comparison with those of humans and other terrestrial mammals. Our results show that chimpanzee muscle exceeds human muscle in maximum dynamic force and power output by ∼1.35 times. This is primarily due to the chimpanzee's higher fast-twitch fiber content, rather than exceptional maximum isometric force or maximum shortening velocities. We suggest that muscular performance capabilities declined during hominin evolution in response to selection for repetitive, low-cost contractile behavior.

Author contributions: M.C.O., B.R.U., and P.J.R. designed research; M.C.O., N.B.H., S.G.L., and P.J.R. performed research; M.C.O., B.R.U., and P.J.R. contributed new reagents/analytic tools; M.C.O. analyzed data; and M.C.O., B.R.U., N.B.H., S.G.L., and P.J.R. wrote the paper.

The authors declare no conflict of interest.

This article is a PNAS Direct Submission. J.M.S. is a guest editor invited by the Editorial Board.

[1]To whom correspondence should be addressed. Email: matthewoneill@email.arizona.edu.

This article contains supporting information online at www.pnas.org/lookup/suppl/doi:10.1073/pnas.1619071114/-/DCSupplemental.

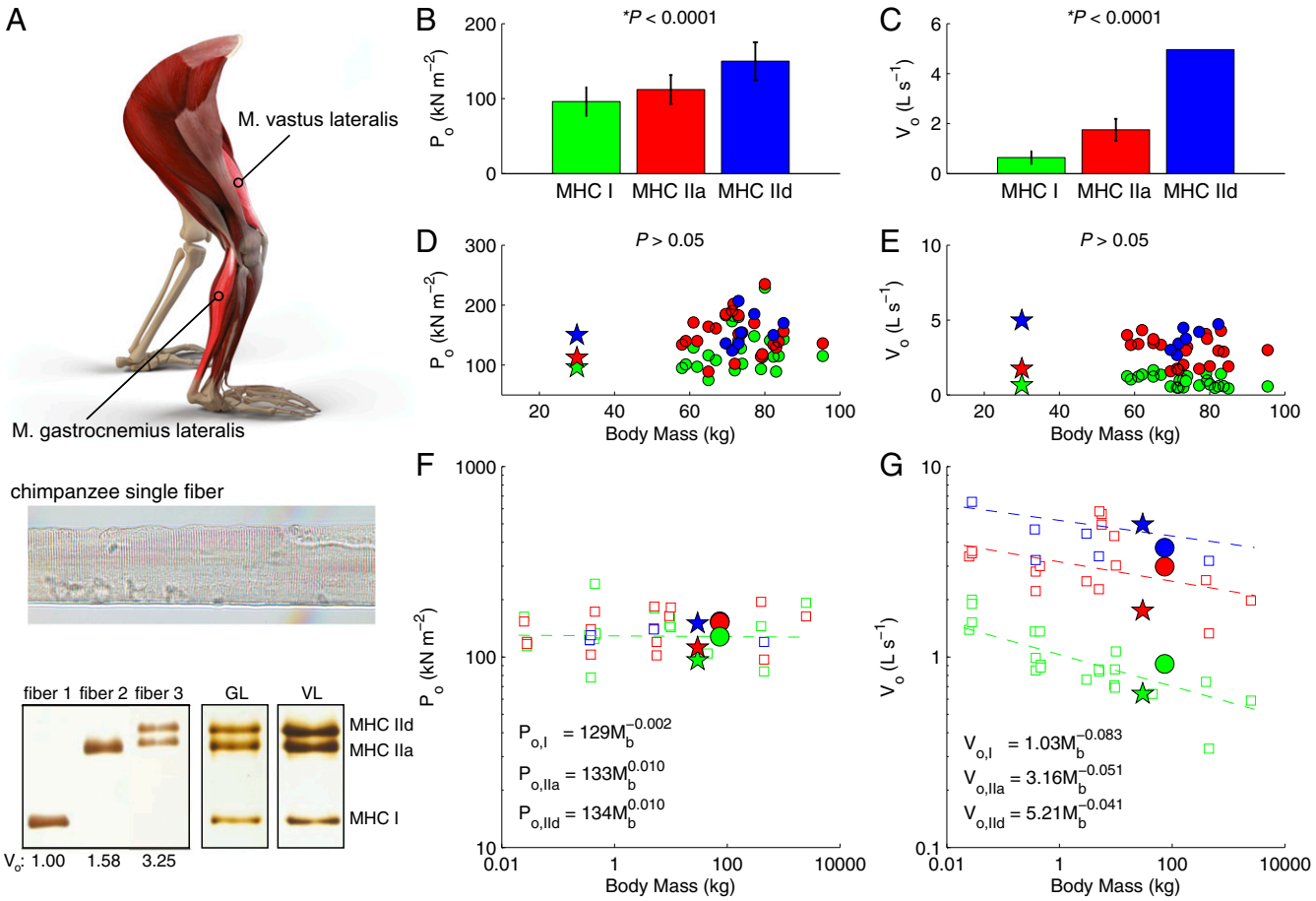

Fig. 1. Muscle contractile properties. (*A*) Chimpanzee single fibers were sampled from *m. vastus lateralis* (VL) and *m. gastrocnemius lateralis* (GL). *Insets* show a chimpanzee single muscle fiber as well as the identification of the fiber MHC isoform content using gel electrophoresis after P_o and V_o measurements. (*B*) The main effect of MHC isoform content on single-fiber P_o; $n = 55$; error bars, SD; *P* value is the result of an ANOVA; $F_{(2,52)} = 21.20$. Paired comparisons indicate that the MHC I ($n = 31$), IIa ($n = 15$), and IId ($n = 9$) P_o samples all differ significantly from each other ($P < 0.05$, Tukey's honest significant difference tests). (*C*) The main effect of MHC isoform content on single-fiber V_o; $n = 22$; error bars, SD; *P* value is the result of an ANOVA; $F_{(2,19)} = 97.16$. Paired comparisons indicated that the MHC I ($n = 14$), IIa ($n = 7$), and IId ($n = 1$ estimate, *SI Appendix, SI Methods*) V_o samples all differed significantly from each other ($P < 0.05$, one-sample *t* tests). (*D* and *E*) The mean P_o and V_o of chimpanzee (stars) muscle compared with human (circles) muscle; *P* values are the results of one-sample *t* tests. (*F* and *G*) The size scaling of P_o and V_o across mammals ranging in mass from 0.01 kg (mouse) to 2,500 kg (rhino) for MHC I, IIa, and IId. Dashed lines are pGLS regression lines of P_o and V_o against body mass by MHC isoform.

and *SI Appendix*, *SI Methods* and Tables S1 and S2). These results, which are taken to be representative of limb and trunk skeletal muscle in general, indicate that chimpanzee muscle is similar to humans and other terrestrial mammals in its single-fiber contractile properties (Fig. 1 *D* and *E*). Indeed, the P_o and V_o of chimpanzee muscle are not significantly different from humans ($P > 0.05$, one sample *t* test) and are generally consistent with expectations based on body size scaling (Fig. 1 *F* and *G*). Given these cellular-level results, humans and chimpanzees can be expected to exhibit commonalities in the molecular properties that affect single-fiber performance, such as actin–myosin kinetics.

We measured the distribution of MHC isoforms within 35 pelvis and hind-limb muscles of chimpanzees and found a balanced distribution of MHC I, IIa, and IId on average (Fig. 2 and *SI Appendix*, Table S3). This is in marked contrast to humans, who exhibit a significant bias toward MHC I fibers in these same muscles and throughout the limbs and trunk overall (14, 15). Although the genetic basis of skeletal muscle MHC isoform specification is an active area of research (e.g., ref. 16), the magnitude of the chimpanzee–human contrast in MHC I fibers appears to exceed the more modest shifts that may be induced through intense athletic training (~10–15%) (17, 18). Furthermore, characterization of fiber-type distributions in the muscles of lemurs, galagos, and macaques suggests that a predominance of MHC II (IIa + IId) isoforms (i.e., fast fibers) is common among primates, as well as other terrestrial mammals (*SI Appendix*, *SI Methods* and Table S5). Indeed, the slow loris (*Nycticebus coucang*) is the only other mammal measured to date with a predominance of slow fibers across its skeletal muscles. Thus, we suggest that the high percentage of MHC I fibers in human skeletal muscle is a derived trait within the hominin lineage, rather than a characteristic of African apes or other nonhuman primates in general.

A salient architectural difference between chimpanzee and human skeletal muscle is that chimpanzees have longer muscle fibers (both in absolute and relative length) (19). Longer muscle fibers have a broader force–length relation that may enhance the dynamic force, work, and power capabilities of a muscle–tendon unit (20). Therefore, to estimate the net interacting effects of P_o, V_o, MHC distribution, and muscle fiber length on maximum dynamic muscle force and power output in vivo, we designed Hill-type "chimpanzee muscle" and "human muscle" models that reflected the parameter differences measured herein and elsewhere (14, 15, 19). Using computer simulations, we determined the maximum dynamic force and power-producing capabilities of these models at the whole-muscle level.

Simulation of a single-burst maximal contraction against a heavy, inertial load predicted that chimpanzee muscle would have

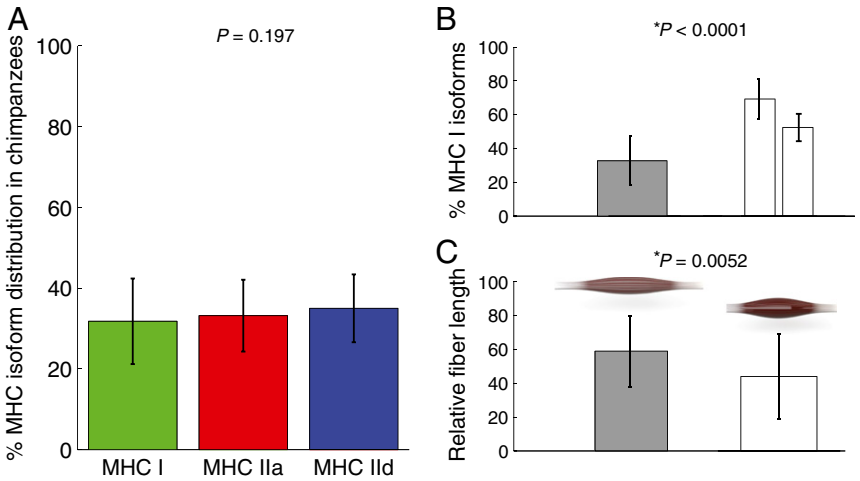

Fig. 2. MHC isoform distributions and average fiber length of chimpanzee and human skeletal muscles. (*A*) Chimpanzees exhibit a balanced distribution of the three MHC isoforms across 35 skeletal muscles (*SI Appendix*, Table S3). *P* value is the result of an ANOVA [$F_{(2,111)} = 1.339$, $P = 0.197$]. (*B*) For the same muscles, humans exhibit a significant bias toward slow-twitch fibers in their skeletal muscle with measurements ranging from (*i*) 69.2 ± 11.7% (14) [$t_{(72)} = 14.04$, $P < 0.0001$, *t* test] to (*ii*) 52.6 ± 7.9% (15) [$t_{(73)} = 9.29$, $P < 0.0001$, *t* test]. This is in contrast to 31.5 ± 11.4% in chimpanzees. (*C*) Chimpanzee muscle fibers also constitute a greater percentage of their total muscle–tendon unit length than do human muscle fibers (i.e., $[L_o/(L_o + L_s)]\cdot 100$, C: 59.0 ± 0.21; H: 44.0 ± 0.25) (23, 24) [$t_{(84)} = 2.87$, $P = 0.0052$, *t* test].

a 1.35 times higher maximum dynamic force [chimpanzee (C): 125.6 $kN\cdot m^{-2}$; human (H): 93.0 $kN\cdot m^{-2}$] and power (C: 220.7 $W\cdot kg^{-1}$; H: 163.8 $W\cdot kg^{-1}$) output than human muscle (Fig. 3). Similarly, simulation of a series of cyclical contractions predicted a 1.34 times higher maximum power output from chimpanzee muscle when the control variables governing muscle excitation and contractile frequency were optimized (C: 172.9 $W\cdot kg^{-1}$; H: 129.2 $W\cdot kg^{-1}$). These results suggest that the larger fraction of MHC II fibers and the longer muscle fiber lengths characteristic of chimpanzee skeletal muscle will increase their dynamic force and power-producing capabilities overall. If a chimpanzee-like or macaque-like phenotype characterized the skeletal muscles of the last common ancestor of chimpanzees and humans, then the maximum dynamic force and power-producing capabilities of hominin skeletal muscles have declined over the past 7–8 million years (13).

Discussion

The 1.35 times differential predicted here seems modest compared with popular accounts of "super strength" in chimpanzees. However, a critical review of the controlled dynamic force- and power-limiting experiments (6–11) that have attempted to quantify this performance differential indicates that, on a mass-specific basis, chimpanzees outperform humans in pulling and jumping tasks by about 1.5 times on average (*SI Appendix, SI Discussion*). Although our simulations do not reproduce the earlier experimental designs in detail, the close approximation of our results to the 1.5 times average suggests that muscle mechanics—MHC isoform content, in particular—accounts for much, but not necessarily all, of the measured chimpanzee–human performance differential. Muscle "static strength," defined as maximum isometric force-producing capabilities (P_o), is not significantly different between these two species and therefore does not contribute to their performance differential (6–8, 10). Of course, linking muscle mechanics to whole-body performance tasks is difficult due to the complexities that arise from the many muscle–tendon units with differing excitations acting across joints with variable leverages. For example, in maximal pulling, chimpanzee performance may benefit from the larger moment arms of some of their fore (upper) limb musculature (19). More detailed musculoskeletal modeling and integrated experimental-simulation work would be required to determine the contributions of these and other possible factors to the remaining 1.15 differential on average. This would also permit a more precise assessment of the contribution of muscle mechanics to the task-specific details that underlie the full range of measured chimpanzee–human performance differentials (i.e., 1.20–2.05 times across studies, *SI Appendix, SI Discussion*).

It has also been hypothesized that humans have greater cortical and/or spinal inhibition of maximal muscle recruitment than chimpanzees, thereby limiting their muscular performance capabilities in comparison (12). If true, this would further increase the chimpanzee–human differential; however, we are unaware of any data that directly support this "inhibition hypothesis." Instead, experimental studies indicate that humans are capable of complete (or near complete) voluntary activation of their musculature when assigned a maximal performance task (e.g., ref. 21). Thus, the expectation that both species are capable of optimizing their neuromuscular control strategies in response to the mechanical demands of a given task appears to be more consistent with available data.

Our integrated experiment-simulation results indicate that the skeletal muscle of chimpanzees is better suited for maximum dynamic force and power output than that of humans, perhaps reflecting the chimpanzee's greater reliance on tree climbing and suspension for survival and fitness. Furthermore, we propose that the higher fraction of MHC I fibers and shorter muscle fiber lengths in human skeletal muscle are adaptive for repetitive, low-cost contractile behavior. MHC I fibers have high mitochondrial volume densities and capillary-fiber contact length (17), which facilitate O_2 diffusion; short fibers can reduce the cost of isometric force output due to a reduction in the muscle volume to cross-sectional area ratio (22). A high fraction of MHC I fibers can also reduce fatigue by limiting the muscle's reliance on glycogen and other intracellular substrates during contractions (17), which permits more frequent muscle activations per day in the aerobic range. Indeed, the large muscle masses (both in absolute and relative terms) in human hind (lower) limbs (19, 23, 24) further enhance our aerobic range during bipedalism (25). Taken together, our results provide an explanation of how chimpanzees can outperform humans in some muscle-driven tasks (e.g., maximal pulling and jumping) (6–11), but not in others (e.g., metabolic cost of walking) (22). Our results may also account for the exceptionally high metabolite concentrations found in human muscle compared with chimpanzee muscle (11).

These data suggest that, although intrinsic muscle contractile properties appear to be conserved, the hominin lineage was characterized by an increase in MHC I isoform content and a decrease in muscle fiber length (19), both of which can impact a range of muscle-driven tasks. The timing of shifts in MHC content and fiber length within the hominin lineage is difficult to establish; however, we anticipate these shifts to have been concurrent with major transitions in locomotor behavior, increases in daily travel distances, increases in home range size, or some combination thereof. The early hominin *Ardipithecus ramidus* is likely similar to chimpanzees and other African apes in its body mass to hind-limb length (26), suggesting that this species still allocated a smaller fraction of its total muscle mass to its hind limbs than humans. The earliest australopithecines (i.e., *Australopithecus anamensis* and

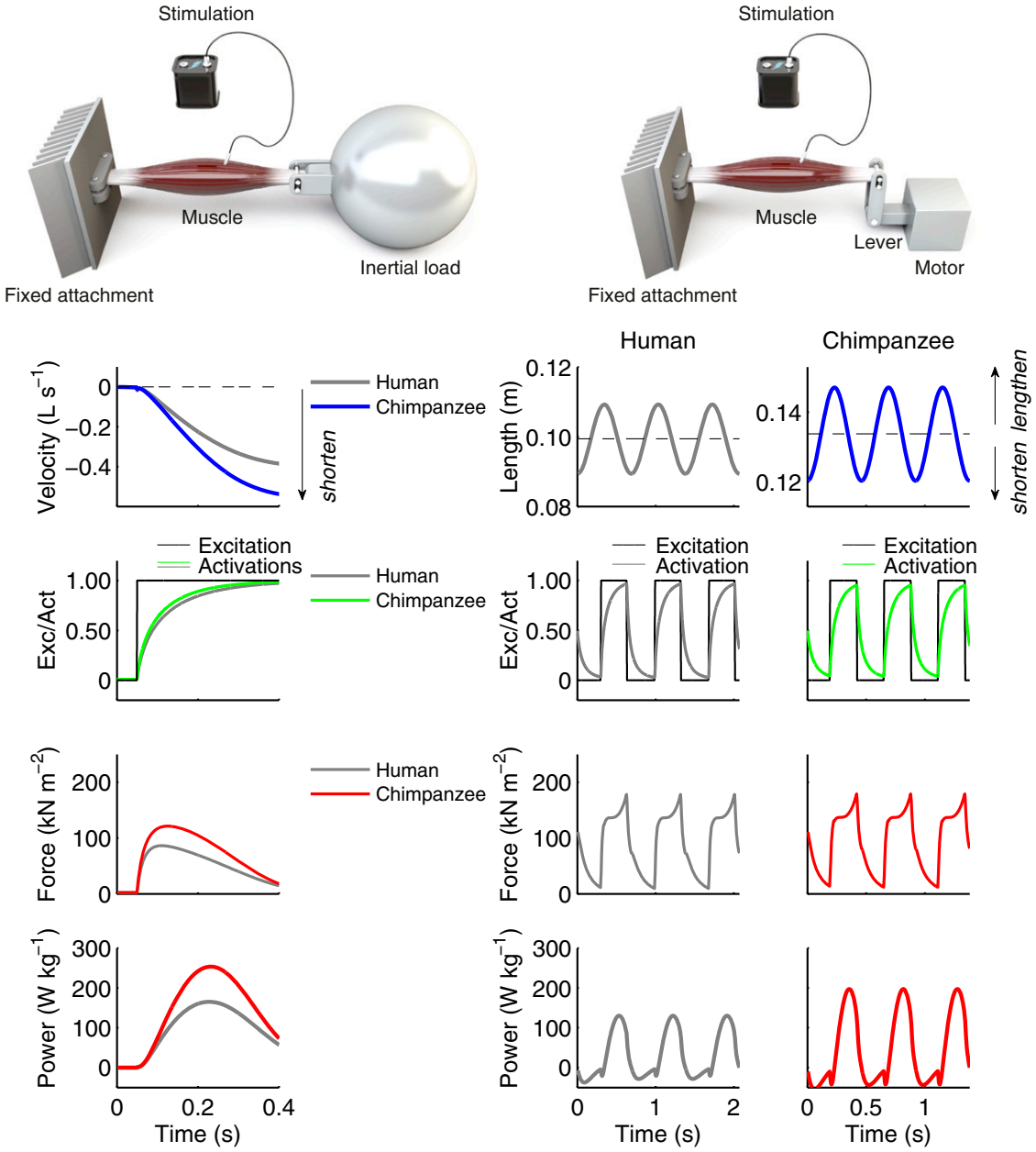

Fig. 3. Muscle model simulations. Single-burst maximal accelerations of an inertial load (first column) and controlled cyclical contractions (second and third columns) were simulated with our chimpanzee muscle and human muscle models. The design of each simulation apparatus is shown at the column top in schematic form with a muscle model affixed in situ. Dashed line is optimal fiber length (L_o). The chimpanzee muscle model generated higher maximum dynamic force and power outputs than the human muscle model under matched simulation conditions.

Australopithecus afarensis) exhibit changes in the pelvis and hindlimb skeleton from *Ar. ramidus* (27, 28), suggesting an adaptive shift toward greater overground locomotion about 4 Mya. However, the proximate ecological trigger for this transition remains elusive (29). By about 1.8 Mya, *Homo erectus* had likely reduced tree climbing to contemporary hunter-gatherer levels while increasing daily travel distances and home range size, perhaps aimed at enhancing diet quality through the inclusion of meat or other low-abundance foods (26, 30, 31).

Contrary to some long-standing hypotheses (6–11), evolution has not altered the basic force, velocity, or power-producing capabilities of skeletal muscle cells to induce the marked differences between chimpanzees and humans in walking, running, climbing, and throwing capabilities (22, 30, 31). This is a significant, but previously untested assumption. Instead, natural selection appears to have altered more global characteristics of muscle tissue, such as MHC distributions and muscle fiber lengths. Our integrated experiment-simulation results indicate that these changes have led to a general reduction in maximum dynamic force and power-producing capabilities; however, they have enhanced metabolic characteristics and endurance capacities of human muscle. Today, intensive athletic training can mitigate some of our inherent limitations in maximal muscle performance, but primarily through force enhancement via skeletal muscle hypertrophy (e.g., ref. 32). More generally, although higher levels of anatomical organization, such as the size and shape of muscle, tendon, and bone have been the main targets of evolutionary processes, hominin muscle dynamic force and power-producing capabilities have also been altered since the *Pan* and *Homo* lineages diverged 7–8 million years ago.

Materials and Methods

Animals. Muscle fibers were sampled from three young male common (*P. troglodytes*) chimpanzees (age: 5.5 ± 0.2 y; mass: 26.5 ± 6.7 kg). All animals were housed in an American Association of Animal Laboratory Care International accredited space with facilities that allowed them to engage in normal social and locomotor behaviors. They had a dedicated animal handler and a staff of technicians who played and interacted with them daily. All of our procedures followed the guidelines of the Stony Brook University Institutional Animal Care and Use Committee.

Muscle Fiber Preparation. Small samples of skeletal muscle (about 1 cm × 0.5 cm × 0.5 cm) were removed from the *musculus* (*m.*) *vastus lateralis* and *m. gastrocnemius lateralis* of the right hind limb of each animal while under general anesthesia. The samples were immediately immersed in cold relaxing solution with 50% (vol/vol) glycerol for overnight transport to The Ohio State University. All of the solutions used for the storage of bundles and measurements of single-fiber contractile properties followed previous experiments (33). Upon arrival, muscle bundles were dissected in a dish containing cold relaxing solution and were stored in fresh relaxing solution with 50% glycerol at −20 °C. Single fibers were subsequently isolated by dissection from the bundles for force and velocity measurements. Single, isolated fibers were mounted in a temperature-controlled experimental chamber, maintained at 15 °C. The fiber was connected at one end to a servo-controlled torque motor (model 322C, Aurora Scientific) and, at the other end, to an isometric force transducer (model 403, Aurora Scientific). The motor and transducer were attached to three-way positioners. The length of the mounted fiber was adjusted by moving the motor or transducer to set the resting striation spacing (i.e., sarcomere length). Striation spacing was determined using a microscope digital camera and image analysis software. Fiber width and depth were measured and fiber cross-sectional area (CSA) was calculated, assuming an ellipsoidal cross-section.

Recording Force and Velocity. The fiber was activated by transferring it to a well in the experimental chamber containing a calcium ion (Ca)-activating solution. The force/pCa (−log[Ca]) relationship was determined in an initial set of fibers to determine the maximally activating solution for subsequent force and velocity measurements. The sarcomere length for these measurements was set to 2.40–2.50 μm. The force/pCa relationship indicated that pCa 4.0 was maximally activating. The active force generated in pCa 4.0 solution was normalized by fiber CSA to calculate the P_o. The V_o was measured using the "slack test" (34). Each fiber was activated during a series of exposures to a pCa 4.0 solution. A known amount of slack was rapidly (within ∼2 ms) introduced into the fiber during each exposure by movement of the motor arm after steady isometric force was attained and the time required to take up the slack was measured from the force record (35). Each fiber was immediately stored at −40 °C until analysis of MHC isoform composition to determine the fiber type.

MHC Isoforms. The MHC isoform(s) expressed in each fiber was identified using SDS/PAGE. The composition, preparation, staining, and densitometric scanning of the gels were identical to those described previously (36). The amount of each MHC isoform in fibers that expressed more than one isoform was calculated as a percentage of the total amount of MHC. The three MHC isoforms that were detected on protein gels were identified by mass spectrometry. MHC gel bands were excised from a Coomassie Blue-stained gel and submitted to the Campus Chemical Instrument Center at The Ohio State University to obtain identification by liquid chromatography–tandem mass spectrometry. The slowest migrating band was identified as fast-type MHC-IId, with a MOWSE score of 27,153, based on 741 peptide matches. The band with intermediate electrophoretic mobility was identified as fast-type MHC-IIa, with a MOWSE score of 23,010, based on 732 peptide matches. The fastest migrating band was identified as slow-type MHC-I, with a MOWSE score of 23,070, based on 694 peptide matches.

The MHC distribution was further determined in samples (10–20 mg) of 35 pelvis and hind-limb muscles from three common chimpanzee specimens not involved in the muscle contractile property measurements. Before each chimpanzee's death (of natural causes), it had been living at a zoo or research institution. The cadaveric remains of each chimpanzee were kept fresh frozen at −20 °C after death until dissection. For each chimpanzee pelvis and/or hind limb, the skin and fascia were removed; individual muscles were identified and dissected free from their attachments. Following the work of others (14), a 2-cm × 0.5-cm × 0.5-cm sample was then taken from each muscle and used to determine MHC isoform composition in the same manner as for the single fibers (*SI Appendix*, Table S3).

Muscle Modeling. Hill-type muscle models were used to investigate the combined effects of P_o, V_o, MHC isoform distributions, and fiber length on maximum dynamic force and power output at the whole-muscle level. The chimpanzee and human models each included species-specific force–velocity, force–length, and activation–deactivation relations, scaled from the generic Thelen2003Muscle (37) model implemented in the OpenSim musculoskeletal modeling environment (38). P_o and V_{max} parameters were assigned the measured P_o and V_o values scaled to normal operating temperature (∼35 °C) (*SI Appendix, SI Methods* and Table S4). The curvature of the force–velocity relationship (A_{rel}) and activation–deactivation time constants (τ_{act}, τ_{deact}) were calculated based on the average fraction of MHC II (fast-twitch) fibers determined for each species (C: 67%, H: 40%) (39). The distribution of fast-twitch fibers in humans represents an average of recent MHC measurements (i.e., MHC IIa+IIx) (14) and older immunohistochemistry measurements [i.e., fast oxidative glycolytic (FOG) + fast glycolytic (FG)] (15). To isolate the effects of muscle on performance, the simulations were conducted using rigid tendons with fiber pennation angles set to 0°. This ensured that the fiber strain matched the muscle–tendon unit strain in the simulations.

A salient architectural difference between chimpanzee and human skeletal muscle is that chimpanzees possess longer muscle fibers on average (19). Chimpanzee (23) and human (24) musculoskeletal models were used to calculate the average relative fiber length [i.e., $L_o/(L_o + L_s)$] for each species and determine the magnitude of the interspecific difference. The two musculoskeletal models include all of the same muscles, except that the human model lacks an *m. obturator externus* and an *m. gluteus maximus superficialis*, which is distinct from the *m. gluteus maximus* in all humans (23). Based on the pelvis and hind-limb muscle–tendon units in the two musculoskeletal models, relative muscle fiber length was 0.59 ± 0.21 in chimpanzees and 0.44 ± 0.25 in humans. This indicates that chimpanzee muscle fibers constitute an ∼15% longer fraction of muscle–tendon unit length on average. We incorporated this difference into our chimpanzee model by increasing relative fiber length from an initial value of 0.43 to a value of 0.58 (*SI Appendix*, Table S4).

Muscle Model Simulations. The performance of each muscle model was simulated under two conditions. For the first condition, the muscle was mounted between a fixed clamp and a mobile, 500-kg inertial load on a frictionless surface (Fig. 3). The inertial load had one degree of freedom, which allowed the muscle to shorten from its optimal length (L_o) thereby accelerating the mass from rest. This simple design approximates the dynamics of a single-burst muscle-powered acceleration, as in a maximal pulling or jumping task. For each muscle model and simulation, the muscle was maximally excited and the dynamic simulation was run for 0.4 ms. The duration of the simulation was sufficient to elicit the maximum dynamic force and power output of each muscle model.

For the second condition, an experimental ergometer was modeled as a muscle mounted between a fixed clamp and mobile clamp on a frictionless surface (Fig. 3). The mobile clamp had one degree of freedom that could be slid to shorten or lengthen the muscle from its L_o. This design was intended to mimic the in vitro preparation used for determining the maximum power-producing capabilities of muscle in cyclical contractions (40). For each muscle model, the mobile clamp was prescribed a sinusoidal motion that shortened and lengthened the muscle by 0.2 L_o, centered on L_o, over three full cycles. This strain amplitude is similar to direct in vivo measurements of muscle fiber strain during a range of high-power output activities (e.g., refs. 41–43). We used a simulated annealing algorithm (44) to optimize a set of control variables that maximized the average net power of the last full strain cycle. Specifically, the control variables included the muscle excitation on (t_{on}) and off (t_{off}) times, as well as the muscle strain cycle frequency (f).

For each muscle model, the optimization problem was configured and solved using the OpenSim-MATLAB application programming interface (38). Maximum force and power outputs were expressed in $kN \cdot m^{-2}$ and $W \cdot kg^{-1}$, respectively. The muscle area (m^2) and mass (kg) divisors were computed using the new chimpanzee P_o values scaled to normal operating temperature and then weighted by MHC isoform distribution for each species (C: 262 $kN \cdot m^{-2}$; H: 248 $kN \cdot m^{-2}$) (*SI Appendix, SI Methods* and Table S4). In all simulations, maximum muscle force was fixed at 2255.4 N, which approximates a human *m. vastus lateralis* (24).

Statistics. Measurements of the single-muscle-fiber contractile properties (i.e., P_o, V_o) of chimpanzees were evaluated for the effect of MHC isoform composition using an analysis of variance (ANOVA) with pairwise comparisons between MHC isoforms. The chimpanzee single-muscle-fiber properties were then compared with similar data for humans and other mammals culled from published studies of single muscle fibers at 15 °C. The human dataset includes a range of populations and ages (*SI Appendix*, Table S1), with human subject

data from our laboratory falling well within this range (*SI Appendix*, *SI Methods* and Fig. S2); the mammalian dataset ranges in size from mice (0.025 kg) to rhinos (2,500 kg) (*SI Appendix*, Table S2). One-sample *t* tests were used to compare the chimpanzee P_o and V_o means to the human mean values from the literature. The scaling relationships of $\log_{10} P_o$ and V_o with $\log_{10}$ body mass were evaluated using phylogenetic generalized least squares (pGLS). The phylogenetic structure of the analyzed species was taken from published mammalian trees (45–47). The pGLS parameters were estimated using the Comparative Analyses of Phylogenetics and Evolution in R package (48) with the parameter lambda (λ) fixed at 0 (star phylogeny) and 1 (Brownian motion) and empirically estimated using a maximum-likelihood (ML) approach. The three different model fits (i.e., $\lambda = 0$, 1, ML) were compared using a likelihood-ratio test. In all cases, the log-likelihood ratio test indicated that $\lambda = 0$ (star phylogeny) provided a statistically equivalent fit to the other two models and therefore was our preferred model for size scaling of all mammalian single-muscle-fiber contractile properties.

The distribution of MHC isoforms within 35 pelvis and hind-limb muscles of chimpanzees (*SI Appendix*, Table S3) was compared using an ANOVA. Independent sample *t* tests were used to conduct pairwise comparisons between the average fraction of MHC I or slow-twitch fibers in chimpanzees and humans, as well as between the relative muscle fiber length in chimpanzees and humans. For the MHC I content and relative fiber-length comparisons, the same 35 muscles were compiled for the chimpanzee and human samples, with the exceptions that *m. gluteus minimus* MHC content was not reported in Tirrell et al. (14) and *m. obturator externus* fiber length was not included in Arnold et al. (24). Exclusion of these muscles from the chimpanzee samples did not alter the statistical significance of the *t*-test results.

ACKNOWLEDGMENTS. We thank Dr. T. Zimmerman, J. Rooney, K. Lasek, E. Moyer, and L. Yohe for assistance with data collection; B. Demes and D. Schmitt for providing chimpanzee cadaveric material; C. Rose for muscle model illustrations; S. Zack for helpful input on mammalian phylogenetics; and M. Miller and J. Stern for comments on earlier versions of the manuscript. Funding was provided by the National Science Foundation (BCS-0935321 to M.C.O. and S.G.L. and BCS-0935327 to B.R.U.).

1. Doran DM (1993) Comparative locomotor behavior of chimpanzees and bonobos: The influence of morphology on locomotion. *Am J Phys Anthropol* 91:83–98.
2. Susman RL, Stern JT, Jr (1982) Functional morphology of *Homo habilis*. *Science* 217: 931–934.
3. Ruff CB, Trinkaus E, Holliday TW (1997) Body mass and encephalization in Pleistocene Homo. *Nature* 387:173–176.
4. Shea JJ (2006) The origins of lithic projectile point technology: Evidence from Africa, the Levant, and Europe. *J Archaeol Sci* 33:823–846.
5. Marlowe FW (2005) Hunter-gatherers and human evolution. *Evol Anthropol* 14:54–67.
6. Bauman JE (1923) The strength of the chimpanzee and orang. *Sci Mon* 16:432–439.
7. Bauman JE (1926) Observations on the strength of the chimpanzee and its implications. *J Mammal* 7:1–9.
8. Finch G (1943) The bodily strength of chimpanzees. *J Mammal* 24:224–248.
9. Edwards WE, Clarke TE (1965) Study of monkey, ape, and human morphology and physiology relating to strength and endurance, phase IX: The strength testing of five chimpanzee and seven human subjects. (Holloman Air Force Base, New Mexico 6571st Aeromedical Research Laboratory, Holloman, NM).
10. Scholz MN, D'Août K, Bobbert MF, Aerts P (2006) Vertical jumping performance of bonobo (*Pan paniscus*) suggests superior muscle properties. *Proc Biol Sci* 273:2177–2184.
11. Bozek K, et al. (2014) Exceptional evolutionary divergence of human muscle and brain metabolomes parallels human cognitive and physical uniqueness. *PLoS Biol* 12: e1001871.
12. Walker A (2009) The strength of great apes and the speed of humans. *Curr Anthropol* 50:229–234.
13. Langergraber KE, et al. (2012) Generation times in wild chimpanzees and gorillas suggest earlier divergence times in great ape and human evolution. *Proc Natl Acad Sci USA* 109:15716–15721.
14. Tirrell TF, et al. (2012) Human skeletal muscle biochemical diversity. *J Exp Biol* 215: 2551–2559.
15. Yamaguchi GT, Sawa AGU, Moran DW, Fessler MJ, Winters JM (1990) Appendix: A survey of human musculotendon actuator parameters. *Multiple Muscle Systems: Biomechanics and Movement Organization*, eds Winters JM, Woo SL-Y (Springer, New York), pp 717–773.
16. Reyes NL, et al. (2015) Fnip1 regulates skeletal muscle fiber type specification, fatigue resistance, and susceptibility to muscular dystrophy. *Proc Natl Acad Sci USA* 112:424–429.
17. Schiaffino S, Reggiani C (2011) Fiber types in mammalian skeletal muscles. *Physiol Rev* 91:1447–1531.
18. Wilson JM, et al. (2012) The effects of endurance, strength, and power training on muscle fiber type shifting. *J Strength Cond Res* 26:1724–1729.
19. Thorpe SKS, Crompton RH, Günther MM, Ker RF, McNeill Alexander R (1999) Dimensions and moment arms of the hind- and forelimb muscles of common chimpanzees (*Pan troglodytes*). *Am J Phys Anthropol* 110:179–199.
20. Caldwell GE (1995) Tendon elasticity and relative length: Effects on the Hill two-component muscle model. *J Appl Biomech* 11:1–24.
21. Kent-Braun JA, Le Blanc R (1996) Quantitation of central activation failure during maximal voluntary contractions in humans. *Muscle Nerve* 19:861–869.
22. Sockol MD, Raichlen DA, Pontzer H (2007) Chimpanzee locomotor energetics and the origin of human bipedalism. *Proc Natl Acad Sci USA* 104:12265–12269.
23. O'Neill MC, et al. (2013) A three-dimensional musculoskeletal model of the chimpanzee (*Pan troglodytes*) pelvis and hind limb. *J Exp Biol* 216:3709–3723.
24. Arnold EM, Ward SR, Lieber RL, Delp SL (2010) A model of the lower limb for analysis of human movement. *Ann Biomed Eng* 38:269–279.
25. Weibel ER, Bacigalupe LD, Schmitt B, Hoppeler H (2004) Allometric scaling of maximal metabolic rate in mammals: Muscle aerobic capacity as determinant factor. *Respir Physiol Neurobiol* 140:115–132.
26. Pontzer H (2012) Ecological energetics in early *Homo*. *Curr Anthropol* 53:S346–S358.
27. Lovejoy CO, Suwa G, Spurlock L, Asfaw B, White TD (2009) The pelvis and femur of *Ardipithecus ramidus*: The emergence of upright walking. *Science* 326:71e1–71e6.
28. Ward C, Leakey M, Walker A (1999) The new hominind species *Australopithecus anamensis*. *Evol Anthropol* 7:197–205.
29. White TD, et al. (2006) Asa Issie, Aramis and the origin of *Australopithecus*. *Nature* 440:883–889.
30. Bramble DM, Lieberman DE (2004) Endurance running and the evolution of *Homo*. *Nature* 432:345–352.
31. Roach NT, Venkadesan M, Rainbow MJ, Lieberman DE (2013) Elastic energy storage in the shoulder and the evolution of high-speed throwing in *Homo*. *Nature* 498:483–486.
32. D'Antona G, et al. (2006) Skeletal muscle hypertrophy and structure and function of skeletal muscle fibres in male body builders. *J Physiol* 570:611–627.
33. Reiser PJ, Welch KC, Jr, Suarez RK, Altshuler DL (2013) Very low force-generating ability and unusually high temperature dependency in hummingbird flight muscle fibers. *J Exp Biol* 216:2247–2256.
34. Edman KA (1979) The velocity of unloaded shortening and its relation to sarcomere length and isometric force in vertebrate muscle fibres. *J Physiol* 291:143–159.
35. Reiser PJ, Moss RL, Giulian GG, Greaser ML (1985) Shortening velocity in single fibers from adult rabbit soleus muscles is correlated with myosin heavy chain composition. *J Biol Chem* 260:9077–9080.
36. Bicer S, Reiser PJ (2004) Myosin light chain 1 isoforms in slow fibers from global and orbital layers of canine rectus muscles. *Invest Ophthalmol Vis Sci* 45:138–143.
37. Thelen DG (2003) Adjustment of muscle mechanics model parameters to simulate dynamic contractions in older adults. *J Biomech Eng* 125:70–77.
38. Delp SL, et al. (2007) OpenSim: Open-source software to create and analyze dynamic simulations of movement. *IEEE Trans Biomed Eng* 54:1940–1950.
39. Umberger BR, Gerritsen KGM, Martin PE (2003) A model of human muscle energy expenditure. *Comput Methods Biomech Biomed Engin* 6:99–111.
40. Josephson RK (1985) Mechanical power output from striated muscle during cyclic contraction. *J Exp Biol* 114:493–512.
41. Olson JM, Marsh RL (1998) Activation patterns and length changes in hindlimb muscles of the bullfrog Rana catesbeiana during jumping. *J Exp Biol* 201:2763–2777.
42. Askew GN, Marsh RL (2001) The mechanical power output of the pectoralis muscle of blue-breasted quail (*Coturnix chinensis*): The in vivo length cycle and its implications for muscle performance. *J Exp Biol* 204:3587–3600.
43. Kurokawa S, Fukunaga T, Fukashiro S (2001) Behavior of fascicles and tendinous structures of human gastrocnemius during vertical jumping. *J Appl Physiol (1985)* 90:1349–1358.
44. Goffe WL, Ferrier GD, Rodgers J (1994) Global optimization of statistical functions with simulated annealing. *J Econom* 60:65–99.
45. Meredith RW, et al. (2011) Impacts of the Cretaceous Terrestrial Revolution and KPg extinction on mammal diversification. *Science* 334:521–524.
46. Springer MS, Murphy WJ, Eizirik E, O'Brien SJ (2003) Placental mammal diversification and the Cretaceous-Tertiary boundary. *Proc Natl Acad Sci USA* 100:1056–1061.
47. Springer MS, et al. (2012) Macroevolutionary dynamics and historical biogeography of primate diversification inferred from a species supermatrix. *PLoS One* 7:e49521.
48. Orme D, Freckleton RP, Thomas G, Petzoldt T, Fritz SA (2011) Caper: Comparative analyses of phylogenetics and evolution in R. Available at r-forge.r-project.org/projects/caper. Accessed September 2015.